NMR Evidence of Sequence Specific DNA Binding by a Cobalt(III)−Bleomycin Analogue with Tethered Acridine

Jennifer D. Tan, Edgardo T. Farinas, Sheila S. David, and Pradip K. Mascharak*,†

Department of Chemistry and Biochemistry, University of California, Santa Cruz, California 95064

Received October 29, 1993[⊗]

Attachment of acridine-9-carboxamido-*N'*-(3-propyl)imidazole (**8**, Int-A) to the Co(III) complex of a designed ligand PMAH that mimics the metal-binding domain of the antitumor drug bleomycin (BLM) has afforded the hybrid molecule [Co(PMA)(Int-A)]Cl_2 (**7**). This structurally characterized compound inflicts DNA strand scission under UV light much like the Co(III)−BLMs. It has been shown previously that UV irradiation of the [Co(PMA)]$^{2+}$ unit gives rise to a ligand-based radical which, in aqueous medium, rapidly collapses into •OH radical, the species actually responsible for the DNA photocleavage observed with the [Co(PMA)X]$^{n+}$ complexes. In this paper we report that attachment of the intercalator acridine to the DNA-cleaving [Co(PMA)]$^{2+}$ unit not only allows the resulting hybrid molecule **7** to bind to DNA quite strongly but also results in preferential DNA photocleavage at 5′GG−N3′ sites. Specific interactions between **7** and the DNA substrate have been studied by high-field NOESY and COSY experiments using the self-complimentary oligonucleotide [d(GATCCGGATC)]$_2$ (**9**) which contains a GG−N site. Intercalative interaction between the acridine moiety of **7** and the duplex **9** is indicated by both broadening and upfield shifts of the acridine protons in the **7**−**9** (1:1) complex. Specific NOEs between the nonexchangeable base protons and the sugar protons of **9** also demonstrate that the acridine moiety of **7** intercalates into the G−G step of **9** and does so (a) with only the outer half (the N-containing side) of the acridine moiety within the base pairs and (b) from the major groove side of the duplex. Interestingly, no intermolecular NOE between the protons of the [Co(PMA)]$^{2+}$ unit of **7** and those of **9** is observed in the NOESY spectra of the **7**−**9** (1:1) complex. Also, the resonances of the [Co(PMA)]$^{2+}$ unit are strongly affected by the salt concentration. The latter two observations indicate that the [Co(PMA)]$^{2+}$ unit of **7** binds to the phosphate backbone of **9** via electrostatic interaction. The products of photocleavage of radiolabeled **9** with **7** suggest that the acridine moiety of **7** binds to the G−G site of **9** and allows photodamage at the GG−N sites by the tethered [Co(PMA)]$^{2+}$ unit.

Introduction

The bleomycin (BLM, **1**) family of glycopeptide antitumor antibiotics is used in combination chemotherapy against several types of cancer.[1] The drug inflicts strand breaks in cellular DNA in presence of metal ions like Fe^{2+} and molecular oxygen.[2−6] Though the kinetically inert Co(III) chelates of BLM (Co(III)−BLMs, **2**) do not inflict DNA damage under normal aerobic conditions,[7] it has recently been reported that Co(III)−BLMs do cleave DNA under UV or visible light,[8−10] and this photoinduced strand scission reaction is indifferent to the presence of dioxygen.[11] To date, there has been no X-ray crystallographic information on metallobleomycins (M−BLMs). As part of our effort toward elucidation of the structures of the Co(III)−BLMs and the mechanism(s) of the light induced DNA strand cleavage reaction, we have synthesized a designed ligand PMAH (**3**, H is the dissociable amide H) that resembles the metal-chelating portion of BLM (boxed area in **1** in Chart 1) and have reported the syntheses and structures of [Co(PMA)-(H_2O)]$(NO_3)_2$ (**4**), [Co(PMA)Cl]Cl (**5**), [Co(PMA)(*N*-MeIm)]-$(NO_3)_2$ (*N*-MeIm = *N*-methylimidazole) (**6**), as good models for the so-called brown, green, and orange forms of Co(III)−BLM.[12] Our results have shown that UV-illumination of **4**−**6** results in the formation of a ligand-based radical that rapidly collapses into hydroxyl radical in aqueous solutions. The latter species is presumably responsible for the DNA strand scission. Though the [Co(PMA)X]$^{n+}$ complexes have been extremely helpful in establishing the mechanism of the unusual mode of DNA photodamage by the Co(III)−BLMs, there exists a notable difference between the model complexes and the Co(III) chelates of the drug. Since the positively charged model complexes bind to DNA solely through electrostatic interactions, they cleave DNA less efficiently compared to the Co(III)−BLMs, which bind to DNA quite strongly (10^6 M^{-1}) through electrostatic interactions as well as intercalation and/or minor groove binding

† Alfred P. Sloan Research Fellow, 1993−1995.

⊗ Abstract published in *Advance ACS Abstracts,* August 1, 1994.

(1) Blum, R. H.; Carter, S. K.; Agre, K. A. *Cancer* **1973**, *31*, 903−914.
(2) Petering, D. H.; Byrnes, R. W.; Antholine, W. E. *Chem.-Biol. Interact.* **1990**, *73*, 133−182.
(3) Stubbe, J.; Kozarich, J. W. *Chem. Rev.* **1987**, *87*, 1107−1136.
(4) Hecht, S. M. *Acc. Chem. Res.* **1986**, *19*, 383−391.
(5) Sugiura, T.; Takita, T.; Umezawa, H. *Met. Ions Biol. Syst.* **1985**, *19*, 81−108.
(6) Dabrowiak, J. C. *Adv. Inorg. Biochem.* **1983**, *4*, 69−113.
(7) DeRiemer, L. H.; Meares, C. F.; Goodwin, D. A. Diamanti, C. I. *J. Med. Chem.* **1979**, *22*, 1019−1023.
(8) Saito, I.; Morii, T.; Sugiyama, H.; Matsuura, T.; Meares, C. F.; Hecht, S. M. *J. Am. Chem. Soc.* **1989**, *111*, 2307−2308.
(9) Subramanian, R.; Meares, C. F. *J. Am. Chem. Soc.* **1986**, *108*, 6427−6429.
(10) Chang, C.-H.; Meares, C. F. *Biochemistry* **1982**, *21*, 6332−6334.
(11) Chang, C.-H.; Meares, C. F. *Biochemistry* **1984**, *23*, 2268−2274.
(12) Tan, J. D.; Hudson, S. E.; Brown, S. J.; Olmstead, M. M.; Mascharak, P. K. *J. Am. Chem. Soc.* **1992**, *114*, 3841−3853.
(13) Bailly C.; Sun J.-S.; Colson, P.; Houssier C.; Hélène, C.; Waring, M. J.; Hénichart J.-P. *Bioconjugate Chem.* **1992**, *3*, 100−103.
(14) Kuroda, R.; Shinomiya, M. *Acta Crystallogr.* **1992**, *C48*, 512−515.
(15) Bowler, B. E.; Ahmed, K. J.; Sundquist, W. I.; Hollis, L. J.; Whang, E. E.; Lippard, S. J. *J. Am. Chem. Soc.* **1989**, *111*, 1299−1306.
(16) Sun, J.-S.; Francois, J.-C.; Montenay-Garestier, T.; Saison-Behmoaras, T.; Roig, V.; Thuong, N. T.; Hélène C. *Proc. Natl. Acad. Sci. U.S.A.* **1989**, *86*, 9198−9202.
(17) Dervan, P. B. *Science* **1986**, *232*, 464−471.
(18) Bowler, B. E.; Hollis, L. S.; Lippard, S. J. *J. Am. Chem. Soc.* **1984**, *106*, 6102−6104.

0020-1669/94/1333-4295$04.50/0

Chart 1

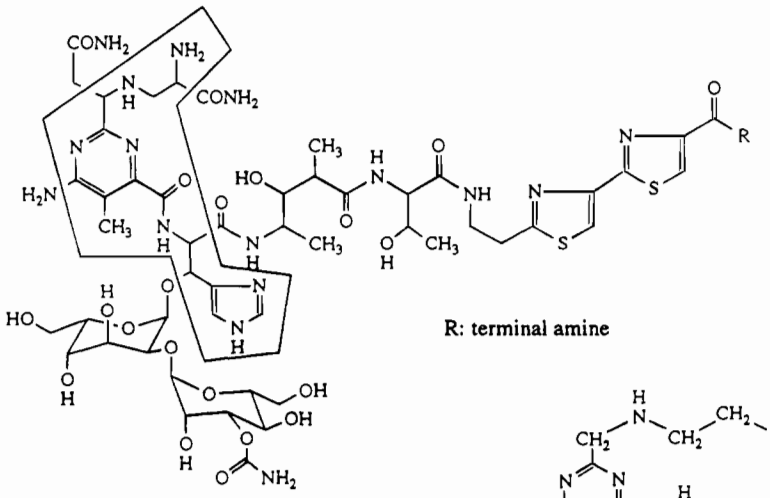

R: terminal amine

BLEOMYCIN (1, BLM)

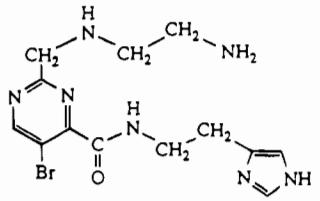

PMAH (3)

of the bithiazole moiety of BLM.[2,3] We therefore, decided to modify the $[Co(PMA)X]^{n+}$ complexes further to enhance their DNA-binding capacity.

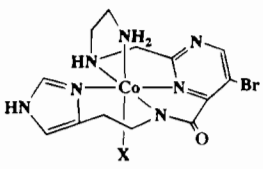

$[Co^{III}(PMA)X]^{n+}$

X = H_2O, n = 2 (4)
X = Cl^-, n = 1 (5)
X = N-MeIm, n = 2 (6)
X = Int-A, n = 2 (7)

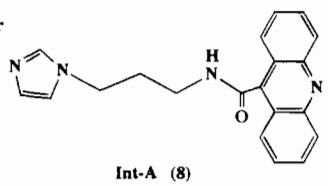

Int-A (8)

In recent years, several accounts on enhanced DNA binding and site-specific cleavage by covalently-linked multifunctional conjugate molecules have appeared.[13-18] Along this line, we have now synthesized and structurally characterized a hybrid molecule $[Co(PMA)(Int\text{-}A)]Cl_2$ (**7**)[19] where Int-A = acridine-9-carboxamido-*N'*-(3-propyl)imidazole (**8**). Acridine was chosen as the DNA-binding group because of its high affinity toward DNA as well as its well-studied intercalation behavior.[20,21] We have already reported the synthesis, structure, and spectroscopic properties of **7**. The efficiency of DNA strand scission by this hybrid complex is a few orders of magnitude higher than observed for the $[Co(PMA)X]^{n+}$ complexes. For example, irradiation of covalently closed circular (ccc) ΦX174 DNA in the presence of 500 μM $[Co(PMA)(N\text{-MeIm})](NO_3)_2$ (**6**) and 10 μM $[Co(PMA)(Int\text{-}A)]Cl_2$ (**7**) showed similar extent of strand scission. Indeed, the capacity of DNA photodamage of **7** approaches that of Co(III)−BLMs under similar experimental conditions. This fact prompted us to investigate whether the increased cleavage efficiency of **7** is also accompanied by site specificity much like the Co(III)−BLMs which preferentially cleave pyrimidine residues located at the 3′ side of guanines.[11] In this paper, we report that cleavage experiments with radiolabeled 266- and 391-bp restriction fragments of pBR322 reveal preferential DNA strand scission by **7** at 5′GG−N3′ sites. We have also performed high-field two-dimensional (2D) NMR experiments, namely nuclear Overhauser effect spectroscopy (NOESY) and *J*-correlated spectroscopy (COSY) to study the specific interactions of **7** with a designed self complimentary oligonucleotide, [d(GATCCGGATC)]$_2$ (**9**), that contains a GG−N site. The NOESY experiments have shown that the acridine moiety of **7** does intercalate into the oligonucleotide and occupies the position between G6 and G7 more often than the other base pairs. In order to verify whether such binding leads to the sequence specific photoscission, additional DNA cleavage experiments have been performed with radiolabeled **9**. Analysis of the photocleavage products by high-resolution polyacrylamide gel electrophoresis demonstrates that the acridine moiety of the hybrid molecule **7** binds to the G−G site of the oligomer and induces photodamage to the GG−N sites.

Experimental Section

The complexes $[Co(PMA)(N\text{-MeIm})](NO_3)_2$ (**6**) and $[Co(PMA)(Int\text{-}A)]Cl_2$ (**7**) were synthesized by following published procedures.[12,19] Blenoxane (bleomycin sulfate) was a gift from the Cetus Corp. Co(III)−bleomycins were prepared and purified as described previously.[7,10,22] The plasmid DNAs (ΦX174, pBR322), bacterial alkaline phosphatase, and the restriction enzymes Xma III and Nar I were purchased from Bethesda Research Laboratories. T4 polynucleotide kinase was purchased from the U.S. Biochemical Corp. Enzymatic reactions were performed according to the specified procedures provided by the suppliers. [γ-^{32}P]ATP (specific activity 3000 Ci/mmol) was procured from Amersham. The Long Ranger gel solution was obtained from AT Biochemicals. Nanopure water was used throughout. Reagents for the DNA synthesis and the C_{18} Sep-Pak columns were purchased from Millipore. The 100% and 99.8% D_2O were purchased from the Aldrich Chemical Co.

Synthesis and Purification of the Decamer. The self-complimentary oligonucleotide [d(GATCCGGATC)]$_2$ (**9**) was synthesized on a 15-μmol scale by using the phosphoramidite chemistry on a Milligen/Biosearch Cyclone Plus DNA synthesizer. The oligomer was purified by HPLC on a reverse phase C_{18} column. Excess buffer salts were removed using a C_{18} Sep-Pak column, and the oligonucleotide was converted into the sodium form using ion exchange chromatography.

(19) Farinas, E.; Tan, J. D.; Baidya, N.; Mascharak, P. K. *J. Am. Chem. Soc.* **1993**, *115*, 2996−2997.
(20) Drummond, D. S.; Simpson-Gildemeister, V. F. W.; Peacocke, A. R. *Biopolymers* **1965**, *3*, 135−153.
(21) Peacocke, A. R.; Skerrett, J. N. H. *Trans. Faraday Soc.* **1956**, *52*, 261−279.
(22) Chang, C.-H.; Dallas, J. L.; Meares, C. F. *Biochem. Biophys. Res. Commun.* **1983**, *110*, **3**, 959−966.

The oligonucleotide was then dissolved in 0.5 mL of 50 mM phosphate buffer (pH 7, also contained 10 mM NaCl and 190 μM EDTA) and lyophilized three times with D_2O (99.8% D). Finally, the decamer was dissolved in 0.5 mL of 100% D_2O. Exact concentrations of the duplex samples in 0.5 mL aliquots of D_2O were calculated using the absorbance values at 260 nm and subsequently placed in 5-mm ultraprecision NMR tubes.

Preparation of Radiolabeled DNA fragments. pBR322 DNA was cleaved with the restriction endonuclease Nar I and dephosphorylated by using bacterial alkaline phosphatase. T4 polynucleotide kinase was then employed to phosphorylate the free 5′-OH ends with [γ-^{32}P]ATP. This step was followed by a final treatment with the restriction endonuclease Xma III. The labeled fragments were then separated by preparative gel electrophoresis and the 391-bp and 266-bp long fragments were excised and extracted by the crush and soak method. The sequences of both restriction fragments were determined by the method of Maxam and Gilbert[23] and were verified by comparison with the published sequence of pBR322.[24] Autoradiography was carried out at −70 °C on Kodak XAR-5 film with an intensifying screen. The free 5′-OH end of the oligonucleotide **9** was radiolabeled with [γ-^{32}P]-ATP and T4 polynucleotide kinase. Excess [γ-^{32}P]ATP was removed from the labeled decamer by NENSORB 20 column chromatography. The sequence of **9** was also confirmed by the method of Maxam and Gilbert.

DNA Cleavage Experiments. Reaction mixtures (25 μL total volume) contained ~5 fmol (~4000 cpm) of a 391- or 266-bp end-labeled DNA duplex and 1 μg of cold carrier ΦX174 DNA in 25 mM Tris−borate buffer and 190 μM EDTA (pH = 8). A UV-transilluminator (UVP-TM-36, λ_{max} = 302 nm) was used to irradiate the solutions for 3 h. The samples were placed behind a Corning 5950 filter (cutoff at 290 nm). Similar experiments were carried out with the end-labeled decamer (**9**). The reaction mixtures in these cases each contained ~50 pmol (~50K cpm) of radiolabeled **9** along with 1 μg of cold **9** as carrier and the samples were irradiated for 12 h at 4 °C. The distance between the light source and the samples was 5 cm in all cases. Following irradiation, the samples were lyophilized and redissolved in 10 μL of 98% formamide loading buffer. The samples were then heated to 90 °C for 10 min, quick-chilled on ice, loaded on denaturing (7 M urea) polyacrylamide (12% for the restriction fragments and 20% for **9**) Long Ranger gels, and electrophoresed at 1500 V for 3 h. Non-irradiated controls in each case showed no DNA strand scission in the presence or absence of the cobalt complexes.

NMR Studies. ^{1}H-NMR spectra were obtained at 25 and 50 °C on a Varian 500-MHz Unity Plus spectrometer (interfaced with a Sun OS 4.1.3). TSP (sodium 3-(trimethylsilyl)propionate-2,2,3,3-d_4) was used as the internal standard, and the HOD signal was suppressed with low-power presaturation irradiation to avoid dynamic range problems. The phase-sensitive NOESY experiments were performed in a 5-mm PFG triple resonance probe. The mixing time was 300 ms. A total of 48 scans per increment were collected in hypercomplex data collection mode[25] for 400 increments along the t_1 axis with 2048 data points in the t_2 direction. The COSY experiments were also carried out with 2048 data points along the t_2 axis while, in the t_1 direction, eight scans per increment were collected for a total of 256 increments. All the final matrices were zero-filled and of the size 2K × 2K. A relaxation delay of 1 s was selected for all 2D experiments. The time domain data along the t_2 and t_1 directions were multiplied by sine-bell window functions prior to Fourier transformation.

Results

Sequence Dependent Cleavage. The results of the light induced site specific DNA cleavage reactions by the Co(III) complexes are shown in Figure 1. Panel A exhibits the results for the 266-bp fragment while panel B displays the same for the 391-bp piece. In both panels, the first four lanes (G, A+G, T+C, and C) contain the products of the Maxam−Gilbert sequencing reactions. The next two lanes include the photocleavage products of brown Co(III)−BLM (**2**, 24 μM) and [Co(PMA)(Int-A)]Cl_2 (**7**, 30 μM) respectively. Both Co(III) complexes show significant site specificities although not necessarily at identical sites. Lanes 7 and 8 in both panels show the results of the photocleavage reactions with [Co(PMA)(*N*-MeIm)]$(NO_3)_2$ (**6**, 1 mM) and Int-A (**8**, 30 μM) respectively. These two species show random cleavage at all sites. Figure 1C illustrates the major cleavage sites for **2** (dashed arrows) and **7** (solid arrows). Brown Co(III)−BLM (**2**) preferentially cleaves 5′G—T3′ and 5′G—C3′ sites while with **7**, strand scission is observed predominantly at 5′GG—N3′ sequences. This difference presumably arises from the different DNA-binding groups in **2** (bithiazole) and **7** (acridine). Figure 1 clearly indicates that the covalent attachment of the acridine unit (an intercalator) to the $[Co(PMA)]^{2+}$ moiety engenders site specificity to the hybrid analogue **7**. It is however, interesting to note that **6** or **8** alone exhibits no specificity at all. This observation suggests some form of cooperativity between the DNA-binding and DNA-cleaving domains of the Co(III) species in such photocleavage reactions.

Assignments of the Nonexchangeable Protons of the Designed Oligonucleotide. The self-complimentary oligonucleotide $[d(GATCCGGATC)]_2$ (**9**) was designed to include the preferred site for **7**, namely GG—N within one turn of a DNA helix. The structures and numbering schemes for **7**, **9**, and the DNA bases are collected in Chart 2. The ^{1}H NMR spectrum of **9** with HOD suppression is shown in Figure 2a in which the resonances of the DNA bases and the sugar protons are indicated. Though the 1D spectrum was insufficient for the assignment of all the nonexchangeable protons of the decamer, it demonstrated the purity of the sample that we subjected to the 2D experiments.

The COSY (Figure 2b) and NOESY (Figure 3) spectra of the duplex **9** were analyzed by the standard sequential method[26,27] to assign all the nonexchangeable ^{1}H resonances. In a previous account, part of the assignments of a dodecamer sequence containing the decamer **9** had been incorrectly reported.[28] We have therefore included the complete assignment of **9** in the present report. The COSY spectrum of **9** (Figure 2b) was used to identify (a) the three cytosines which show distinct cross-peaks between their H5 and H6 protons and (b) the two thymines from correlations between their TCH_3 and TH6 protons. These assignments served as the starting point for the sequential method.

Initial NOESY experiments were carried out with two different mixing times, 200 and 300 ms, to evaluate the effect(s) of spin diffusion under long mixing times. Since the spectra with 300 ms mixing time exhibited more intense cross-peaks with no evident sign of spin diffusion, all of the subsequent experiments and spectral assignments were performed with 300 ms mixing time. Figure 3b shows the base to base connectivities along the entire length of **9** while Figures 3c and 3d exhibit the base to H1′ and base to H2′−H2″ sugar correlations respectively, along with resonance assignments for all the nonexchangeable protons involved. Each base proton (H8 or H6) exhibits NOEs to its own sugar H1′ and H2′−H2″ as well as the H1′ and H2′−H2″ protons of its 5′ neighbor. Such connectivities allows an NOE walk from the 5′- to the 3′-end

(23) Maxam, A. M.; Gilbert, W. *Methods Enzymol.* **1980**, *65*, 499−560.
(24) Maniatis T.; Fritsch, E. F.; Sambrook, J. *Molecular Cloning. A Laboratory Manual*; Cold Spring Harbor Laboratory: Cold Spring Harbor, NY, pp 480−487.
(25) States, D. J.; Haberkorn, R. A.; Ruben, D. J. *J. Magn. Reson.* **1982**, *48*, 286-292.
(26) Wüthrich, K. *NMR of Proteins and Nucleic Acids*; John Wiley & Sons, Inc.: New York, 1986.
(27) (a) Scheek, R. M.; Russo, N.; Boelens, R.; Kaptein, R.; van Boom, J. H. *J. Am. Chem. Soc.* **1983**, *105*, 2914−2916. (b) Hare, D. R.; Wemmer, D. E.; Chou, S.-H.; Drobny, G. *J. Mol. Biol.* **1983**, *171*, 319−336.
(28) Kumar, M. R.; Hosur, R. V.; Roy, K. B.; Miles, H. T.; Govil, G. *Biochemistry* **1985**, *24*, 7705−7711.

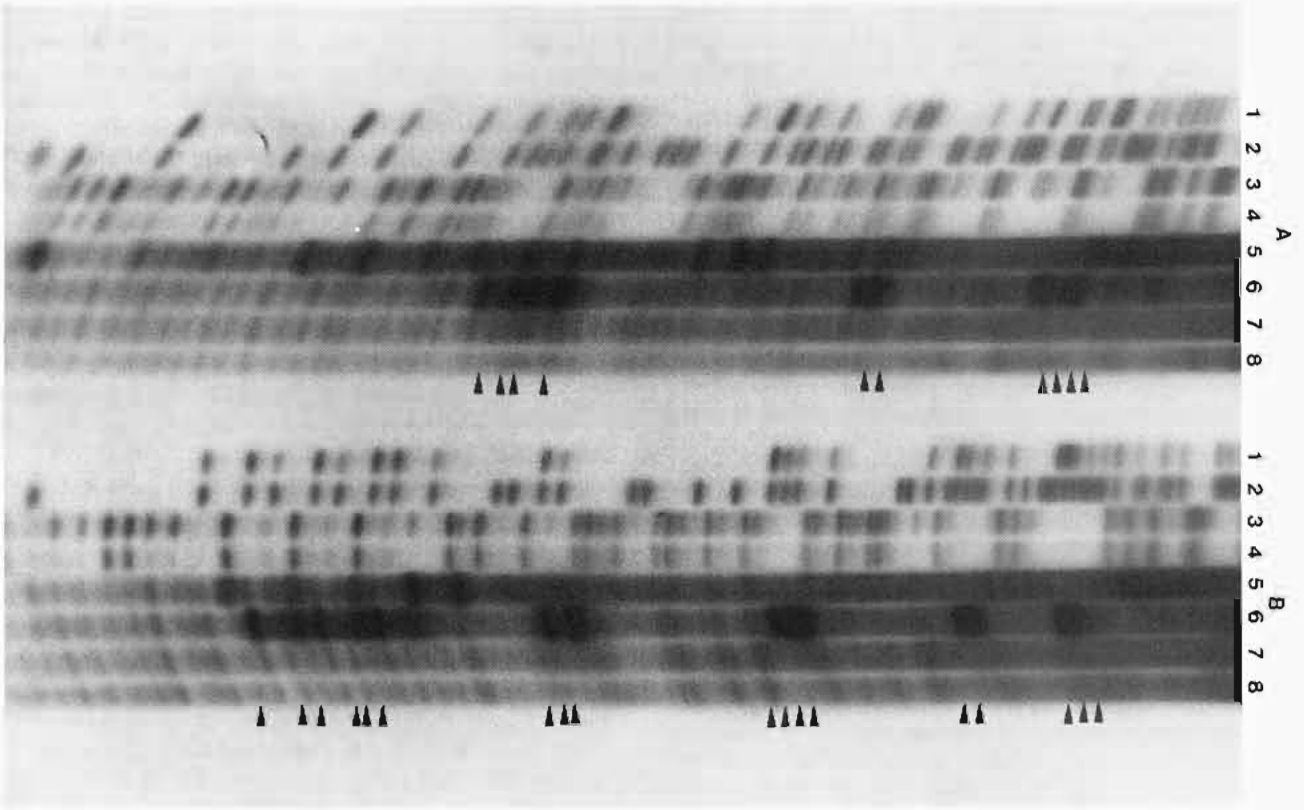

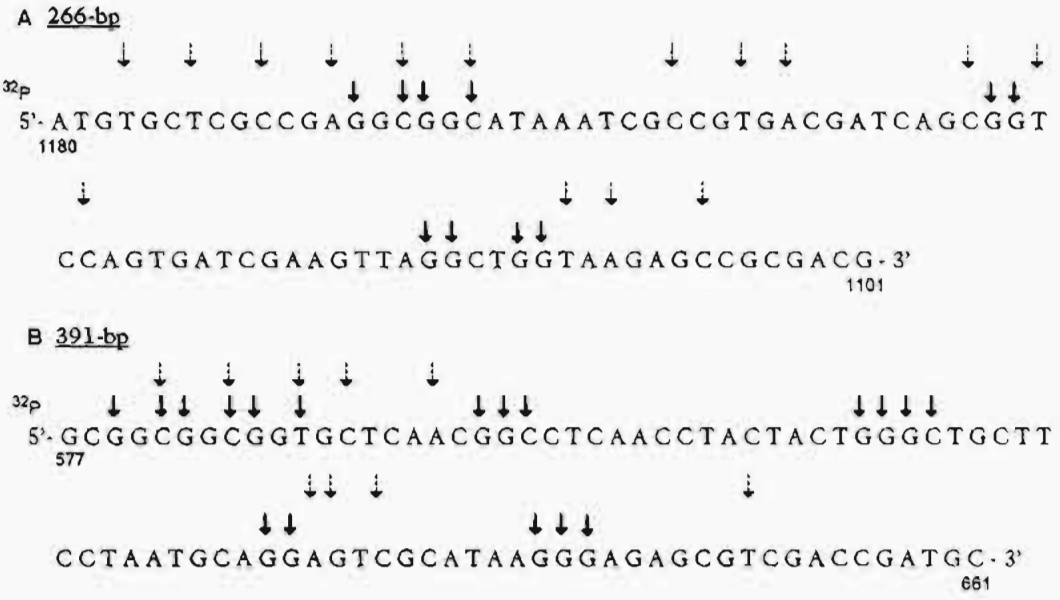

C

Figure 1. Sequence dependent photocleavage of the 5′-end labeled 266-bp (panel A) and 391-bp (panel B) restriction fragments of pBR322 by brown Co(III)−BLM, **6**, **7**, and **8**. Lanes 1−4 contain the products of the Maxam−Gilbert sequencing reactions (G, A+G, C+T, and C respectively). Lanes 5−8 contain the products of reactions between ~5 fmol of 5′-end labeled double stranded restriction fragments (in a total volume of 25 μL of 25 mM Tris−borate, 190 μM EDTA, pH = 8 buffer) and the following compounds: lane 5, 24 μM of brown Co(III)−BLM; lane 6, 30 μM of [Co(PMA)(Int-A)]Cl_2 (**7**); lane 7, 1 mM of [Co(PMA)(*N*-MeIm)]$(NO_3)_2$ (**6**); lane 8, 30 μM of Int-A (**8**). All reaction mixtures contained 1 μg of ΦX174 DNA as carrier and were irradiated at 290 nm for 3 h except for lane 5 which was irradiated for 15 min. Panel C: Cleavage sites observed in the DNA strand scission reaction with [Co(PMA)(Int-A)]Cl_2 (**7**) (solid arrows) and brown Co(III)−BLM (dashed arrows).

of the oligonucleotide. In the present case, such a walk indicates that the decamer **9** is indeed in the B-form.[29] Included in Table 1 are the assignments of the nonexchangeable protons of the decamer duplex **9** at 25 and 50 °C.

^{1}H NMR Spectrum of [Co(PMA)(Int-A)]Cl_2 (7). The ^{1}H NMR spectrum of **7** at 25 °C is shown in Figure 4 and the peak positions along with their assignments (see Chart 2 for the numbering) are listed in Table 2. The assignments were completed with the help of the ^{1}H and ^{13}C spectra, ^{1}H−^{1}H COSY spectra, and ^{13}C−^{1}H COSY spectra (not shown). The resonances of the acridine protons appear between 7 and 8 ppm and the triplet doublet characteristics are clearly visible. The aromatic protons of the coordinated PMA^- framework exhibit peaks at the following positions: imidazole H1, 8.51; imidazole

Chart 2. Structures and Numbering Schemes for $[Co(PMA)(Int\text{-}A)]Cl_2$ (**7**), DNA Base Pairs C-G and T-A, Deoxyribose Sugar, and the Self-Complimentary Duplex $d[GATCCGGATC]_2$ (**9**)

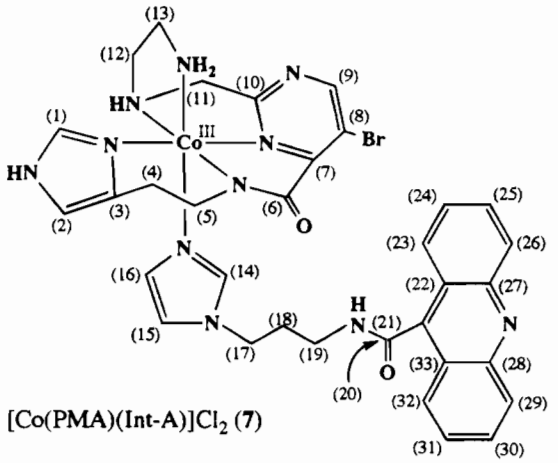

$[Co(PMA)(Int\text{-}A)]Cl_2$ (**7**)

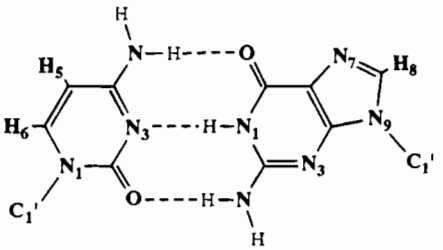

C≡G

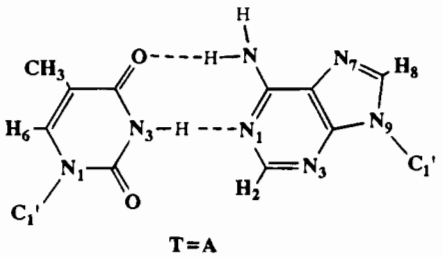

T=A

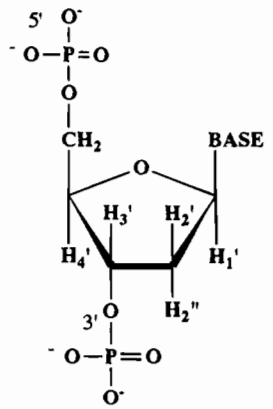

$$\begin{matrix} {}^{5'}\mathbf{G_1\ A_2\ T_3\ C_4\ C_5\ G_6\ G_7\ A_8\ T_9\ C_{10}}{}^{3'} \\ {}^{3'}\mathbf{C_{10}\ T_9\ A_8\ G_7\ G_6\ C_5\ C_4\ T_3\ A_2\ G_1}{}^{5'} \end{matrix} \quad \textbf{(9)}$$

H2, 7.30; pyrimidine H9, 9.17 ppm.[12] The aromatic protons of the imidazole in the tether region resonate at 6.32 (H15), 7.28 (H14), and 7.22 (H16) ppm.

Titration of $[d(GATCCGGATC)]_2$ (9) with 7. The results of the addition of **7** to **9** at 25 °C are shown in Figure 5 (only the aromatic region is illustrated). At substichiometric ratios of **7**, only one set of resonances was observed. This indicated that the spectrum was in the intermediate exchange regime. As the concentration of **7** was raised, the resonances of the oligonucleotide broadened to a significant extent. Furthermore, the resonances of the acridine moiety of **7** did not emerge as sharp as in the free molecule. Nevertheless, there were at least two sharp peaks in the low field region that arise from imidazole H1 and pyrimidine H9 of the PMA^- framework. In the **7**−**9** (1:1) complex, the pyrimidine H9 peak is shifted downfield (9.39 ppm compared to 9.17 ppm in **7**) and the peak for the imidazole H1 appears as a doublet (8.46 and 8.51 ppm). The splitting of the imidazole H1 resonance of **7** into a doublet is also noted when a small amount of **9** (~0.2 equiv) is added to **7**. This splitting most likely results from the differential interaction of the Λ and Δ enantiomers of the $[Co(PMA)]^{2+}$ moiety of **7** with **9**.[30] Since the hybrid molecule **7** interacts with **9** in a somewhat constrained manner due to both intercalative and electrostatic interactions, the oligonucleotide is able to act as a chiral shift reagent for the $[Co(PMA)]^{2+}$ portion of **7** and allows resolution of specific enantiomeric protons. Simple electrostatic binding of **4** to **9** (data not shown) does not result in such doubling of specific resonances of the PMA^- framework. In the **7**−**9** (1:1) complex however, the electrostatic interaction(s) between the $[Co(PMA)]^{2+}$ moiety of **7** and the negative phosphate backbone of the duplex contributes significantly to the overall process of enantiomeric discrimination. This is illustrated by the NMR spectrum of the **7**−**9** (1:1) complex run under a high salt condition (Figure 6). As the NaCl concentration was raised to 1.0 M, the imidazole H1 resonances collapsed into a singlet at 8.51 ppm and the pyrimidine H9 was shifted back to 9.17 ppm, the positions noted for uncomplexed **7**. High concentrations of Na^+ ions clearly diminish the electrostatic portion of the total interaction between **7** and **9**.

Temperature Dependence of the 7−9 (1:1) complex. In order to study the dynamic behavior of the **7**−**9** (1:1) complex and to obtain sharper peaks to aid assignment of all its relevant resonances, the temperature of a sample of **7**−**9** (1:1) complex

(29) Van de Ven, F. J.; Hilbers, C. W. *Eur. J. Biochem.* **1988**, *178*, 1−38.

(30) All the octahedral cobalt complexes containing the pentadentate ligand PMA^- have been isolated as racemic mixtures. In our work so far, we have not separated the Λ and Δ enantiomers of these complexes since the relevant forms of Co−BLMs would also exist as racemic mixtures.

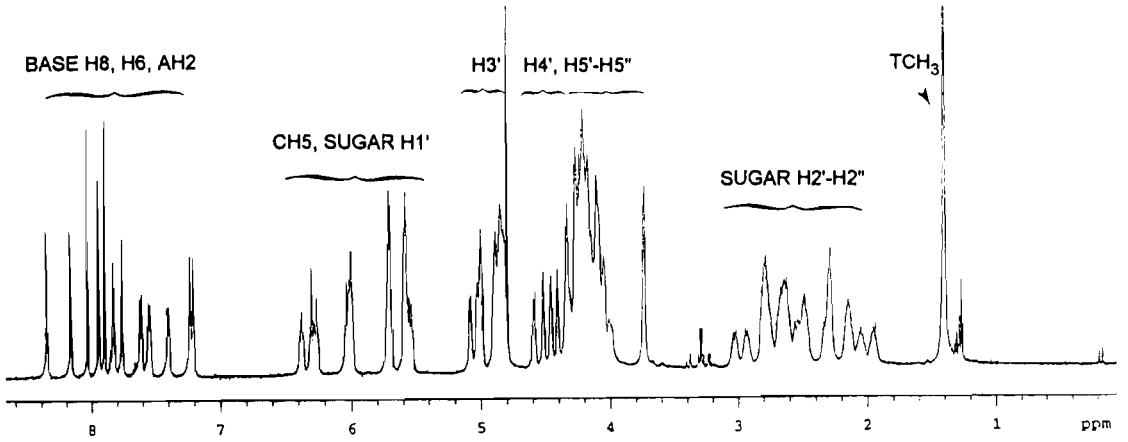

(a)

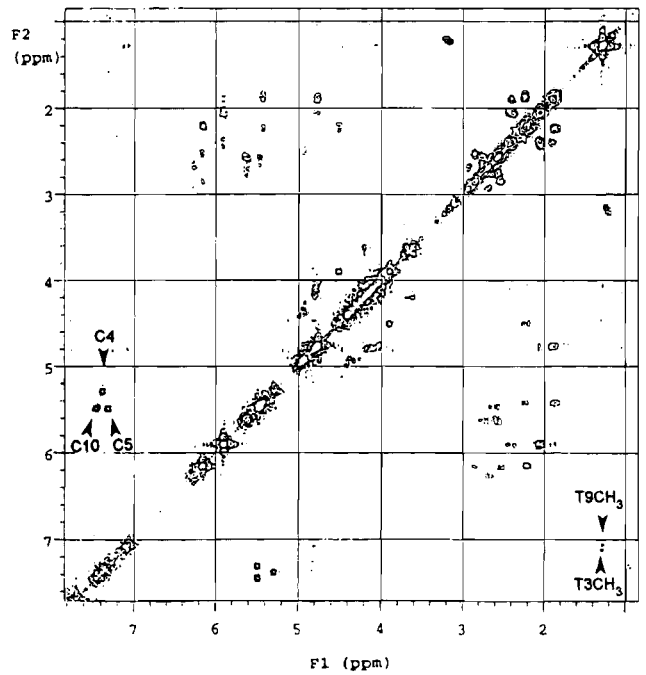

(b)

Figure 2. (a) ^{1}H NMR spectrum (500 MHz) of d[GATCCGGATC]$_2$ (**9**) in D_2O phosphate buffer (pH 7.1) at 25 °C. (b) COSY spectrum of **9** at 25 °C showing correlations between CH5 and CH6 for C4, C5, and C10, as well as between TH6 and TCH_3 for T3 and T9.

was varied in the range of 5−70 °C (Figure 7). At 5 °C, all the resonances were very broad indicating slow to intermediate exchange. Significant sharpening of the peaks was observed when the temperature of the sample reached 70 °C. This implied that **7** was in fast exchange with the duplex at this temperature. The spectrum at 50 °C appeared sharp enough (intermediate to fast exchange regime) for reliable data collection. Also, at temperatures higher than 50 °C, the resonances started to shift downfield more pronouncedly. Therefore, the spectrum at 50 °C was chosen for additional NOESY studies since the spectrum was fairly sharp with no detectable melting of the self-complementary duplex. The chemical shifts for the thymine methyl groups (TCH_3) indicated that **9** was not melted even at 60 °C. The melting curve of the **7**−**9** (1:1) complex also suggested increased stabilization of the duplex in the presence of **7** (data not shown).

Changes in the NMR spectrum of **7**−**9** (1:1) complex with temperature (Figure 7) provide further information regarding the enantioselective interactions between the $[Co(PMA)]^{2+}$ moiety of **7** and **9**. At 25 °C, doubling of the imidazole H1 resonance due to differential interactions of the enantiomeric $[Co(PMA)]^{2+}$ moiety of **7** with **9** is clearly visible while the pyrimidine H9 resonance at 9.39 ppm appears as a broad peak. As the temperature is raised, the H9 peak sharpens, and eventually at 60 °C, two distinct peaks due to the Λ and Δ enantiomers of the $[Co(PMA)]^{2+}$ moiety of **7** are resolved. In the fast exchange regime at higher temperatures, doubling of the H9 resonance is evident due to narrower line widths.

NOESY Spectra of the 7−9 (1:1) Complex: Intramolecular NOEs. NOESY spectra with 300-ms mixing time were recorded at two temperatures (25 and 50 °C) to collect NOE information under different regimes of exchange (Figures 8and 9). At 50 °C, the intramolecular DNA cross-peaks were more distinct compared to those in the broad spectrum at 25 °C. In both set of spectra, an NOE walk from the 5′- to the 3′-end of the oligonucleotide was possible, thus enabling complete assignments for all the nonexchangeable base protons as well as the H1′ and H2′-H2″ protons of **9** in the **7**−**9** (1:1) complex.

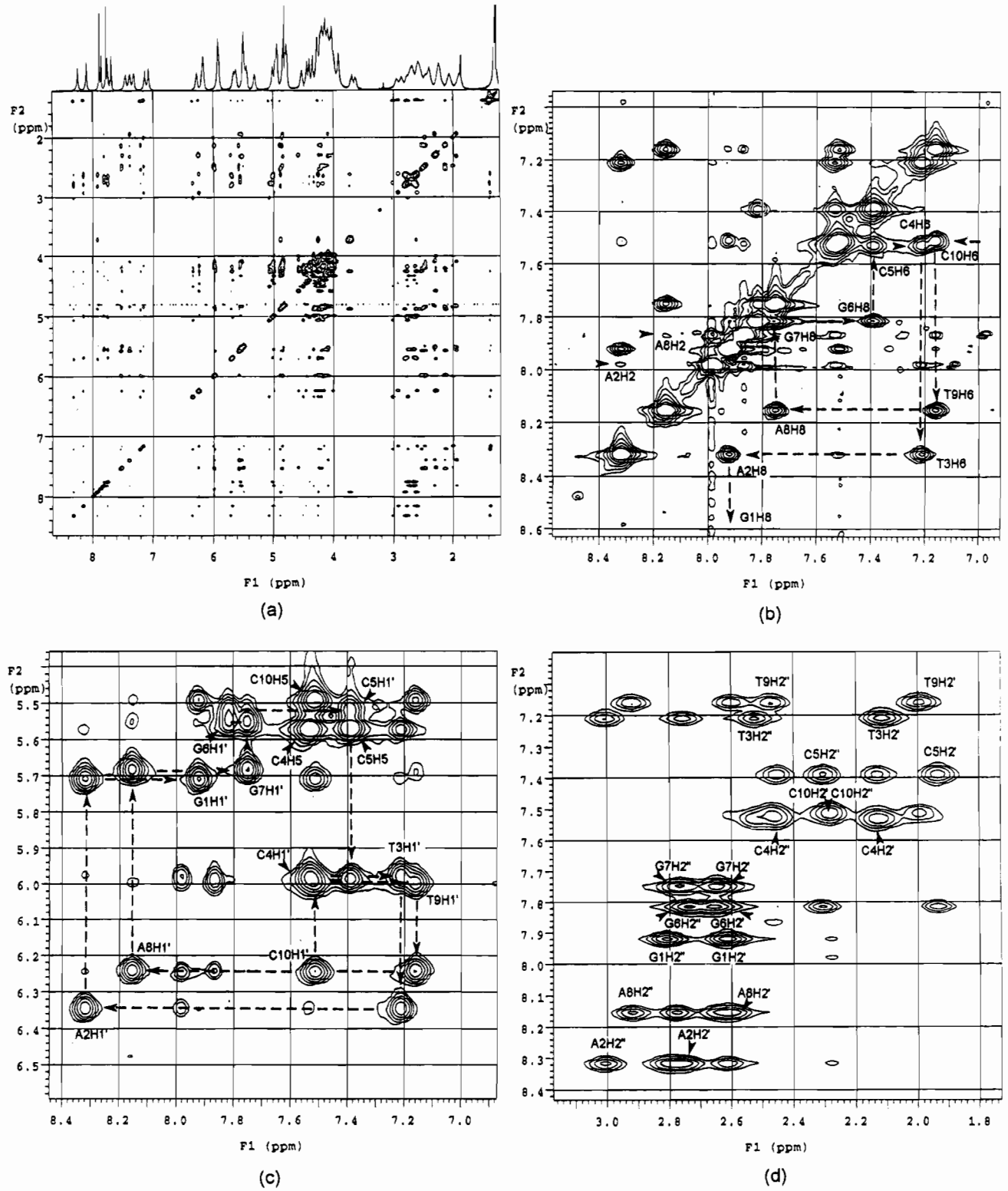

Figure 3. (a) NOESY spectrum (500 MHz) of the duplex d[GATCCGGATC]$_2$ (**9**) at 25 °C in D_2O phosphate buffer (pH = 7.1). (b–d) Expanded NOESY contour plots for **9** showing distance connectivites between the base protons and protons of their own 5′-flanking bases (b), the base protons (6.9–8.4 ppm) and their own sugar H1′ as well as the H1′ sugar protons of their 5′ neighbor (5.4–6.6 ppm) in addition to the CH5–CH6 correlations (c), and the base protons (6.9–8.4 ppm) to their own sugar H2′ and H2″ protons as well as to the H2′–H2″ sugar protons of their 5′ neighbor (5.4–6.6 ppm) (d).

Listed in Table 1 are the resonance assignments (at both temperatures) of **9** together with the shifts upon complexation while Table 2 contains the same for **7**. In the **7**–**9** (1:1) complex, the oligonucleotide resonances are shifted by about 0.1 ppm upfield (denoted by a negative sign, Table 1). Shifts in the oligonucleotide resonances are observed at G7, G6, C5, and C4 which are located at the designed binding site for **7**. This is the 5′G—G3′ region in the decamer where the G6—C5 and G7—C4 are hydrogen bonded in the duplex. The resonances of **7** exhibit comparatively larger magnitude of shifts in the **7**–**9** (1:1) complex (Table 2). Downfield shifts (positive numbers) are noted for protons H2 and H9 of the PMA^- framework while the acridine protons H23 to H32 are moved upfield by as much as 1 ppm. The acridine peaks are also broadened to a significant extent. Furthermore, it is evident from the NOESY spectra (Figures 8 and 9) that half of the acridine protons (residing on

Table 1. ^{1}H NMR Chemical Shifts of Nonexchangeable Protons of d[GATCCGGATC]$_2$ in the Free (**9**) and Bound Form (**7**−**9** Complex) at 25 and 50 °C[a] with Differences in Chemical Shifts upon Complexation (Δ) Also Listed

25 °C		base H6,H8			AH2, CH5, TCH$_3$			sugar H1′			sugar H2′			sugar H2″		
		7 + **9** (1:1)	**9**	Δ	**7** + **9** (1:1)	**9**	Δ	**7** + **9** (1:1)	**9**	Δ	**7** + **9** (1:1)	**9**	Δ	**7** + **9** (1:1)	**9**	Δ
1	G	7.86	7.92	−0.06				5.63	5.71	−0.08	2.54	2.61	−0.07	2.72	2.81	−0.09
2	A	8.26	8.31	−0.05	7.88	8.00	−0.12	6.25	6.35	−0.10	2.72	2.75	−0.03	2.87	3.00	−0.13
3	T	7.18	7.21	−0.03	1.37	1.38	−0.01	5.93	5.98	−0.05	2.08	2.11	−0.03	2.44	2.52	−0.08
4	C	7.48	7.51	−0.03	5.47	5.57	−0.10	5.90	5.99	−0.09	2.08	2.12	−0.04	2.40	2.46	−0.06
5	C	7.35	7.38	−0.03	5.55	5.57	−0.02	5.48	5.51	−0.03	1.90	1.92	−0.02	2.25	2.30	−0.05
6	G	7.77	7.81	−0.04				5.46	5.54	−0.08	2.60	2.66	−0.06	2.72	2.74	−0.02
7	G	7.73	7.74	−0.01				5.57	5.69	−0.12	2.60	2.63	−0.03	2.67	2.78	−0.11
8	A	8.14	8.15	−0.01	7.78	7.87	−0.09	6.17	6.24	−0.07	2.60	2.60	0.00	2.87	2.92	−0.05
9	T	7.14	7.16	−0.02	1.36	1.37	−0.01	5.95	6.00	−0.05	1.99	2.00	−0.01	2.43	2.47	−0.04
10	C	7.47	7.52	−0.05	5.55	5.49	0.06	6.18	6.24	−0.06	2.25	2.28	−0.03	2.25	2.28	−0.03

50 °C		base H6,H8			AH2, CH5, TCH$_3$			sugar H1′			sugar H2′			sugar H2″		
		7 + **9** (1:1)	**9**	Δ	**7** + **9** (1:1)	**9**	Δ	**7** + **9** (1:1)	**9**	Δ	**7** + **9** (1:1)	**9**	Δ	**7** + **9** (1:1)	**9**	Δ
1	G	7.81	7.87	−0.06				5.66	5.70	−0.04	2.45	2.49	−0.04	2.62	2.68	−0.06
2	A	8.27	8.33	−0.06				6.26	6.35	−0.09	2.74	2.78	−0.04	2.91	2.98	−0.07
3	T	7.20	7.24	−0.04	1.41	1.43	−0.02	5.95	6.01	−0.06	2.10	2.14	−0.04	2.46	2.52	−0.06
4	C	7.48	7.56	−0.08	5.59	5.62	−0.03	5.93	6.02	−0.09	2.09	2.14	−0.05	2.40	2.46	−0.06
5	C	7.34	7.41	−0.07	5.58	5.59	−0.01	5.54	5.59	−0.05	1.88	1.92	−0.04	2.24	2.32	−0.08
6	G	7.75	7.80	−0.05				5.49	5.60	−0.11	2.59	2.64	−0.05	2.67	2.72	−0.05
7	G	7.69	7.72	−0.03				5.58	5.69	−0.11	2.58	2.61	−0.03	2.69	2.74	−0.05
8	A	8.12	8.12	0.00				6.20	6.26	−0.06	2.61	2.61	0.00	2.84	2.87	−0.03
9	T	7.18	7.22	−0.04	1.44	1.45	−0.01	6.02	6.08	−0.06	2.08	2.10	−0.02	2.43	2.46	−0.03
10	C	7.63	7.68	−0.05	5.77	5.83	−0.06	6.24	6.30	−0.06	2.28	2.27	0.01	2.28	2.27	0.01

[a] Values in ppm relative to TSP.

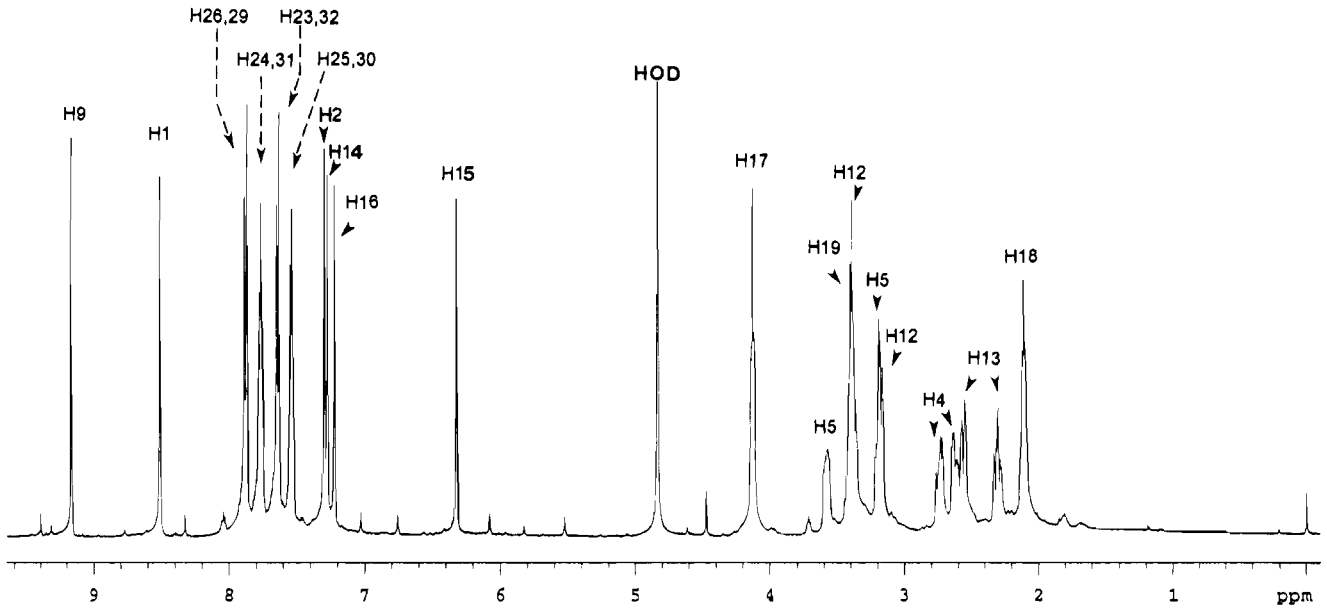

Figure 4. ^{1}H NMR spectrum of [Co(PMA)(Int-A)]Cl$_2$ (**7**) in D_2O phosphate buffer (pH 7.1) at 25 °C. The various signal assigments are indicated.

the side of the N in the ring, ~6.95 ppm region) are more broadened and shifted upfield compared to the other half (peaks in the 7.3 ppm region), a fact suggesting significant intercalative interaction between the N-containing side of the acridine ring system and the duplex.

NOESY Spectra of the 7−9 (1:1) Complex: Intermolecular NOEs. Table 3 presents the intermolecular NOESY cross peaks and their relative intensities observed for the complex **7**−**9** (1:1) at 25 and 50 °C. As expected, more NOEs are observed in the spectra recorded at 25 °C due to slower exchange of **7** with **9**. The strongest correlations appear for the acridine protons of **7** and the G6−G7 region (as well as for C4−C5) of the decamer **9**. Several NOEs also exist for the neighboring base pairs A2−T9 and T3−A8 although their intensities are much weaker than that of the G6−G7 region. There are a number of NOE cross peaks that are consistent with intercalation of the acridine moiety into the G6−G7 step; most notably those between the acridine peaks in the 6.95 ppm region and G6H1′, G7H1′, G6H2″, and G7H2″. Other acridine-to-base NOEs namely, acridine to G7H8, G6H8, C5H5, C4H5, T3CH$_3$, and T9CH$_3$, also indicate intercalative interaction. Interestingly, the acridine peaks in the 7.34 ppm region exhibit NOEs to the T9CH$_3$ and T3CH$_3$, a fact that requires the intercalative interaction to occur in the major groove.

Sequence Dependent Photocleavage of the Oligonucleotide [d(GATCCGGATC)]$_2$ (9) with 7. In order to verify whether conclusions from the NOE experiments are also supported by the products of the photocleavage reactions of **9** by **7**, the light-induced strand scission experiment was performed, and the result is shown in Figure 10. Lane 2 includes the G+A Maxam−Gilbert sequencing fragments while lane 3 contains the products of the reaction of 30 μM of **7** with 1 μg of **9** under UV light for 12 h. The observed strand scission at A8, G6, and C5 is consistent with intercalation of the acridine moiety of **7** at the

Table 2. ^{1}H NMR Chemical Shifts of Nonexchangeable Protons of [Co(PMA)(Int-A)]$(NO_3)_2$ in the Free (**7**) and Bound Form (**7**−**9** Complex) at 25 and 50 °C[a] with Differences in Chemical Shifts upon Complexation (Δ) Also Listed

	25 °C			50 °C			50 °C		
	7 + **9** (1:1)	**7**	Δ	**7** + **9** (1:0.2)	**7**	Δ	**7** + **9** (1:1)	**7**	Δ
H1	8.45, 8.51	8.51	−0.06	8.45, 8.51	8.51	−0.06	8.45, 8.51	8.51	−0.06
H2	7.41, 7.38	7.30	0.11	7.40	7.31	0.09	7.41, 7.39	7.31	0.10
H4	2.75	2.73	0.02	2.70	2.69	0.01	2.71	2.69	0.02
H5	3.48	3.39	0.09	3.45	3.40	0.05	3.44	3.40	0.04
H9	9.39	9.17	0.22	9.35	9.19	0.16	9.35	9.19	0.16
H12	3.27	3.28	−0.01	3.26	3.28	−0.02	3.26	3.28	−0.02
H13	2.47	2.45	0.02	2.45	2.44	0.01	2.45	2.44	0.01.08
H14	7.25	7.28	−0.03	7.27	7.28	−0.01	7.31, 7.27	7.28	0.03
H15	6.20, 6.25	6.32	−0.12	6.24, 6.26	6.32	−0.08	6.24, 6.26	6.32	−0.08
H16	7.25	7.22	0.03	7.27	7.21	0.06	7.31, 7.27	7.21	0.10
H17	4.11	4.13	−0.02	4.10	4.16	−0.06	4.10	4.16	−0.06
H18	2.00	2.03	−0.03	2.02	2.11	−0.09	2.02	2.11	−0.09
H19	2.87	3.41	−0.54	3.24	3.39	−0.15	3.25	3.39	−0.14
H23,32	7.34	7.64	−0.30	7.50	7.72	−0.22	7.36	7.72	−0.36
H24,31	7.34	7.77	−0.43	7.43	7.84	−0.41	7.34	7.84	−0.50
H25,30	6.95	7.54	−0.59	7.20	7.60	−0.40	7.05	7.60	−0.55
H26,29	6.95	7.87	−0.92	7.10	8.00	−0.90	6.98	8.00	−1.02

[a] Values in ppm relative to TSP.

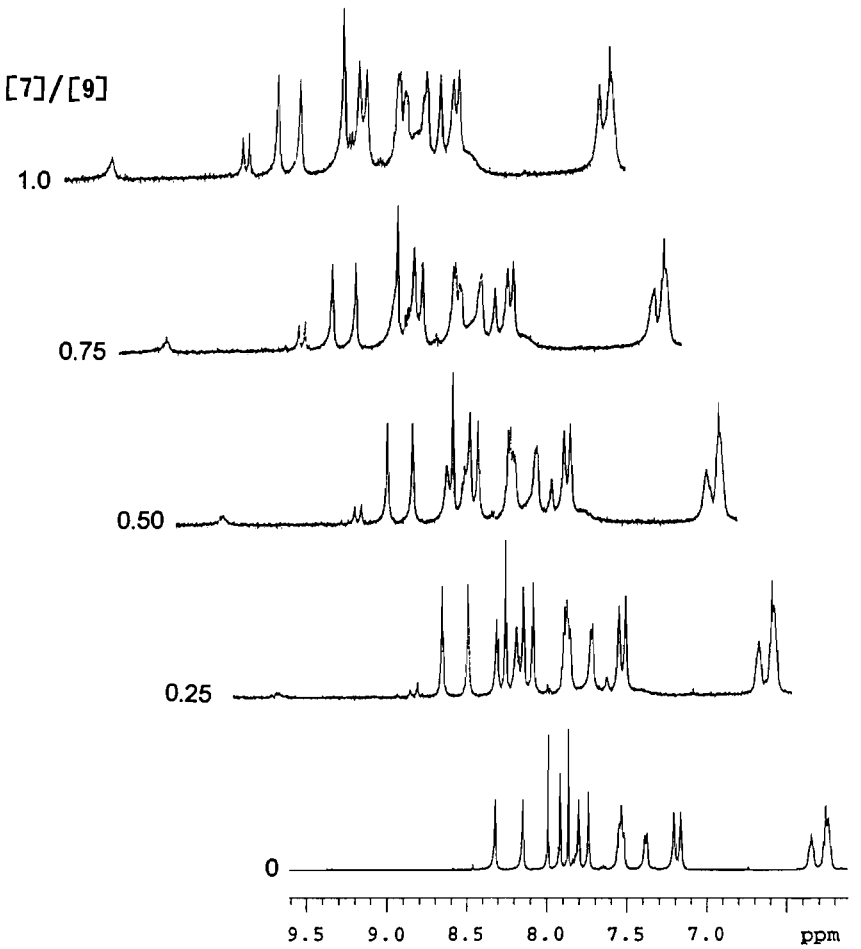

Figure 5. Aromatic region of the ^{1}H NMR spectrum of the [Co(PMA)(Int-A)]Cl_2 (**7**)−d[GATCCGGATC]$_2$ (**9**) complex as a function of the [**7**]/[**9**] ratio in D_2O phosphate buffer (pH = 7.1) at 25 °C.

G6−G7 step of the duplex **9** since the $[Co(PMA)]^{2+}$ unit of **7** is then optimally positioned to cause photodamage at the adjacent sites.

Discussion

Unlike **6** or **8**, the conjugate model [Co(PMA)(Int-A)]Cl_2 (**7**) photocleaves plasmid DNA at specific sites though the site specificity is different from that of Co(III)−BLM (**2**). Both electrophoretograms of Figure 1 show that **7** cleaves predominantly in the GG regions in addition to 5′GG−N3′ sites. The site specificity of **7** is intriguing since covalent attachment of **6** to **8** leads to this property; a simple mixture of **6** and **8** does not exhibit site-specific cleavage. It is known that acridines bind more favorably to GC-rich regions of DNA[31,32] and inflict photodamage to DNA via formation of radicals in the vicinity

(31) (a) Cieplak, P.; Rao, S. N.; Grootenhuis, P. D. J.; Kollman, P. A. *Biopolymers* **1990**, *29*, 717−727. (b) Aggarwal, A.; Islam, S. A.; Kuroda, R.; Neidle, S. *Biopolymers* **1984**, *23*, 1025−1041.
(32) Müller, W.; Crothers, D. M. *Eur. J. Biochem.* **1975**, *54*, 267−277.
(33) Dhar, A.; Chaudhuri, U. *Arch. Biochem. Biophys.* **1974**, *162*, 310−312.

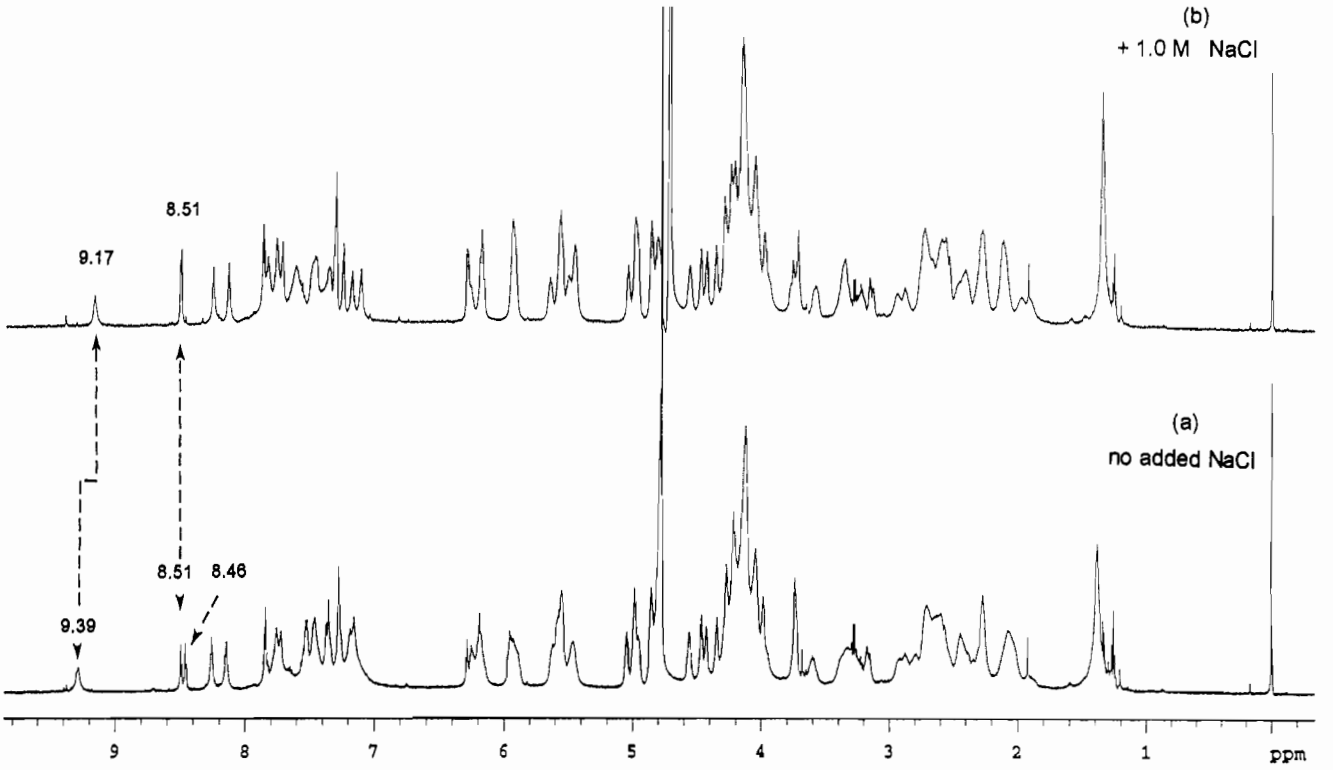

Figure 6. ^{1}H NMR spectrum (25 °C) of the **7**−**9** (1:1) complex as a function of salt concentration: (a) no salt added; (b) 1 M NaCl added.

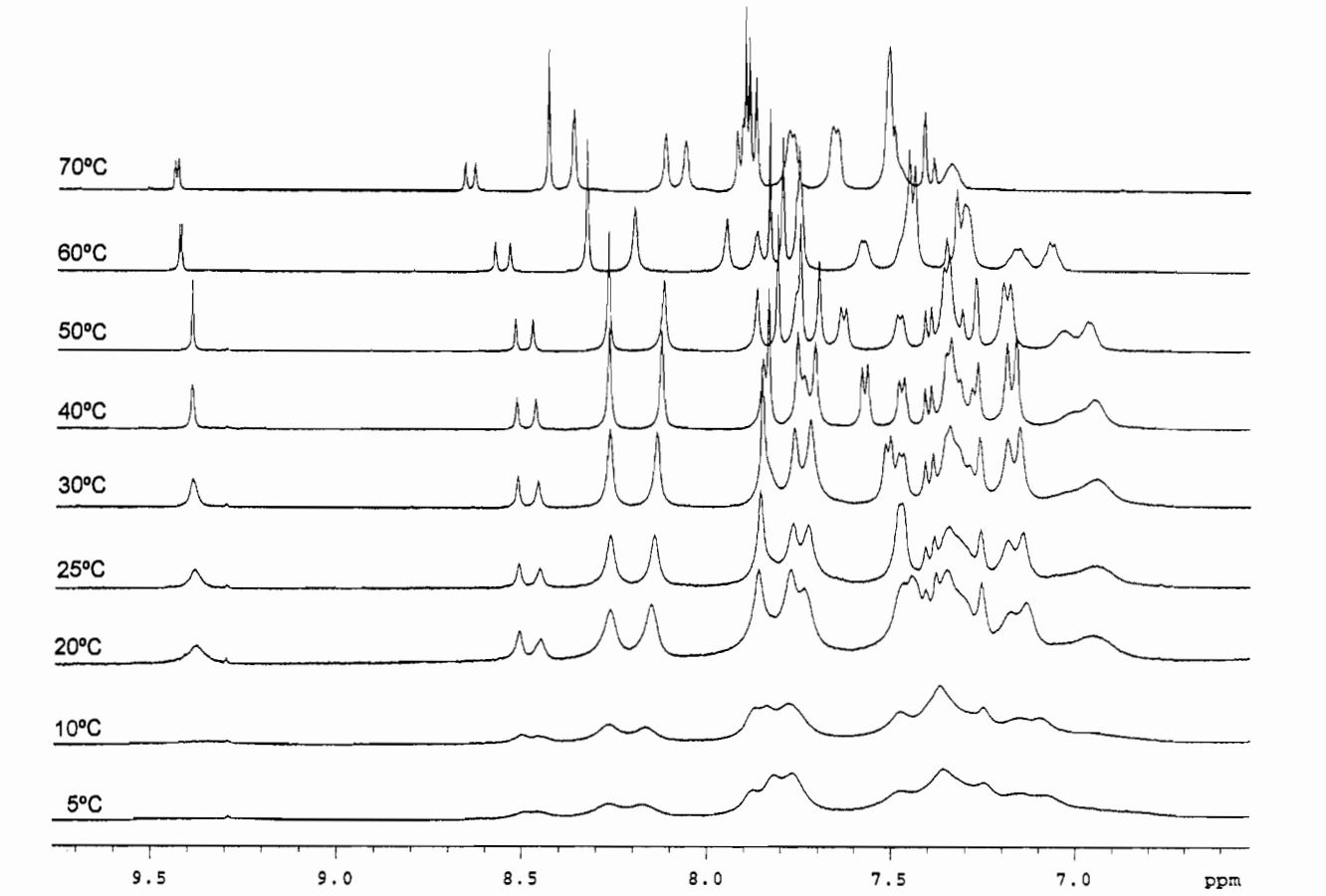

Figure 7. Aromatic region of the ^{1}H NMR spectrum of the **7**−**9** (1:1) complex as a function of temperature.

of the helix.[33−35] However, if the site specificity of **7** relied solely on the acridine moeity, then the ligand Int-A (**8**) should have shown similar cleavage sites. Instead, **8** exhibits only random cleavage (Figure 1). Since [Co(PMA)(*N*-MeIm)]$^{2+}$ (**6**) binds to DNA through electrostatic interaction, it also induces random cleavage of DNA upon UV illumination. It thus appears that the acridine moiety of **7** assists more in selective binding

(34) Gräslund, A.; Rigler, R.; Ehrenberg, A. *FEBS Lett.* **1969**, *4* (3), 227−230.

(35) Kubota, Y.; Miura, M. *Bull. Chem. Soc. Jpn.* **1967**, *40*, 12, 2989.

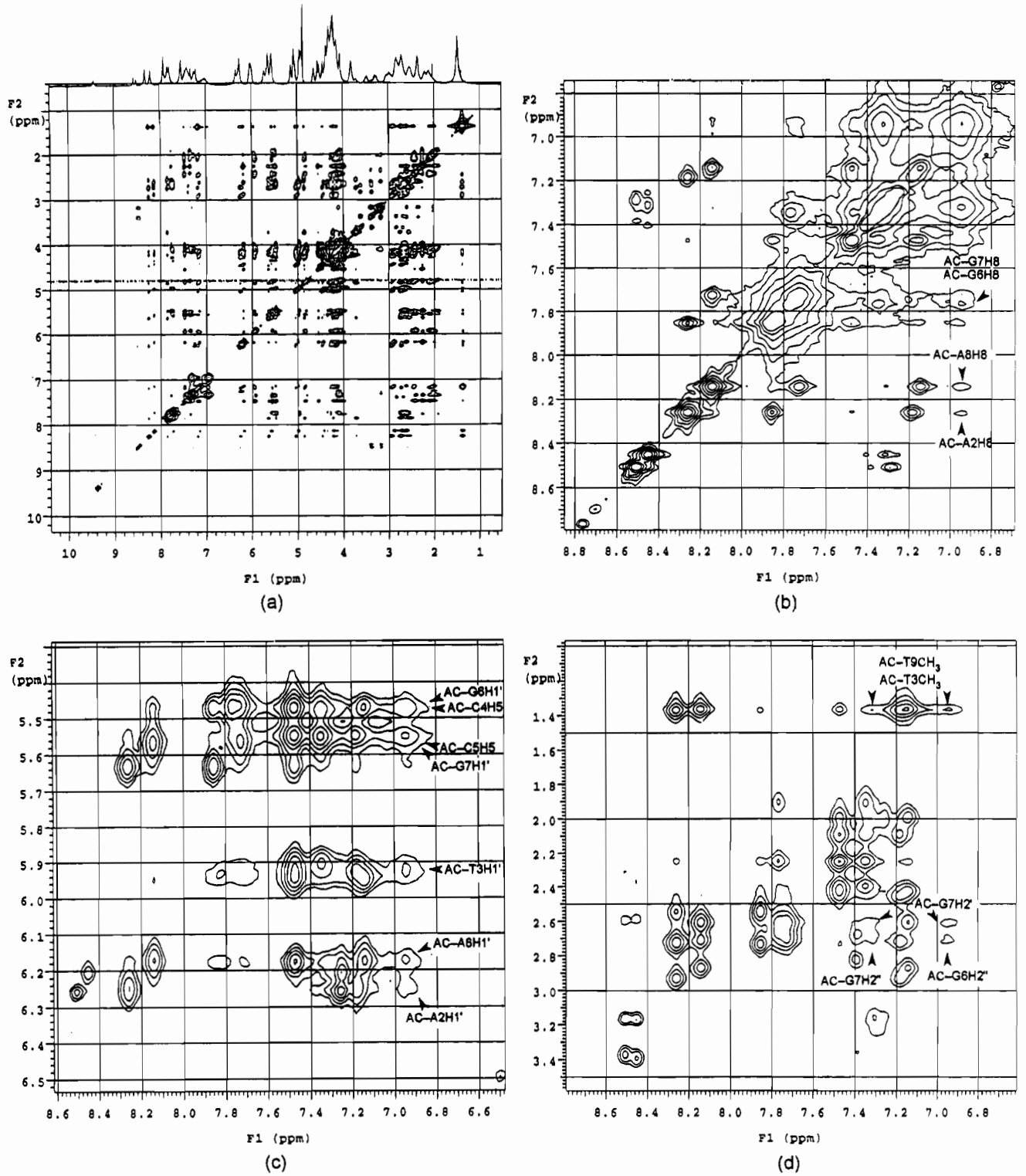

Figure 8. (a) NOESY spectrum (500 MHz) of the **7**−**9** (1:1) complex at 25 °C in D_2O phosphate buffer (pH = 7.1). (b−d) Expanded NOESY contour plots for **9** showing distance connectivites between the base protons and protons of their own 5′-flanking bases (b), the base protons (6.9−8.4 ppm) and their own sugar H1′ as well as the H1′ sugar protons of their 5′ neighbor (5.4−6.6 ppm) in addition to the CH5−CH6 correlations (c), and the base protons (6.9−8.4 ppm) to their own sugar H2′ and H2″ protons as well as to the H2′−H2″ sugar protons of their 5′ neighbor (5.4−6.6 ppm) (d). The intermolecular NOEs listed in Table 3 are indicated.

of the conjugate molecule in the G-rich regions of DNA, and such binding induces site specificity in the otherwise random photocleavage reaction of the tethered $[Co(PMA)]^{2+}$ unit.

Though somewhat broad (Figure 5), the NMR spectrum of the **7**−**9** (1:1) complex at 25 °C provides clear spectroscopic evidence of intimate binding of **7** to **9**. Upon complexation, the acridine peaks of **7** are broadened and move upfield by 0.5−1 ppm (Table 2). These changes are typical of intercalation of the acridine ring into the duplex.[36,37] The peaks corresponding to the protons of the PMA^- framework of **7** remain quite sharp in the spectrum of **7**−**9** (1:1) and also exhibit distinct signs of interaction between the $[Co(PMA)]^{2+}$ unit and the

(36) Mauffret, O.; Rene, B.; Convert, O.; Monique, M.; Lescot, E.; Fermandijian, S. *Biopolymers* **1991**, *31*, 1325−1341.

(37) Laugaa, P.; Delepierre, M.; Dupraz, B.; Igolen, J.; Roques, B. P. *J. Biomol. Struct. Dyn.* **1988**, *6*, **3**, 421−441.

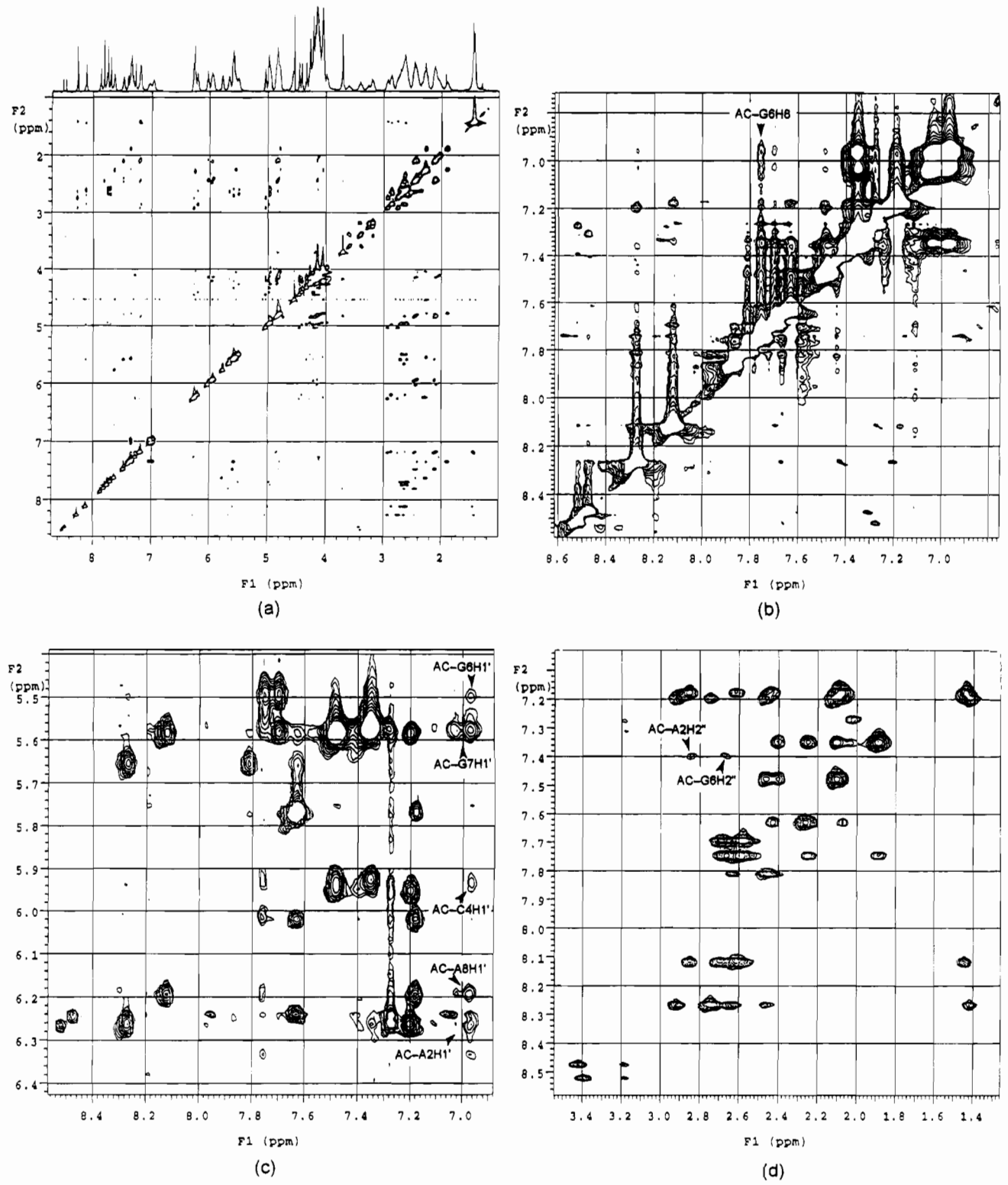

Figure 9. (a) NOESY spectrum (500 MHz) of the **7**−**9** (1:1) complex at 50 °C in D_2O phosphate buffer (pH = 7.1). (b−d) Expanded NOESY contour plots for **9** showing distance connectivites between the base protons and protons of their own 5′-flanking bases (b); the base protons (6.9−8.4 ppm) and their own sugar H1′ as well as the H1′ sugar protons of their 5′ neighbor (5.4−6.6 ppm) in addition to the CH5-CH6 correlations (c); and the base protons (6.9−8.4 ppm) to their own sugar H2′ and H2″ protons as well as to the H2′-H2″ sugar protons of their 5′ neighbor (5.4−6.6 ppm) (d). The intermolecular NOEs listed in Table 3 are indicated.

duplex. For example, the pyrimidine H9 peak moves from 9.17 ppm (in free **7**) to 9.39 ppm in **7**−**9** (1:1). The most interesting change upon duplex binding is the emerging doublet (8.46, 8.51 ppm) from imidazole H1 (Figure 5). Area integration clearly indicates that the doublet corresponds to one proton. Careful examination of the NOESY spectra of **7**−**9** (1:1) reveals that the other imidazole protons (H2, H14, H15, and H16) of **7** also split into doublets (Table 2). Furthermore, doubling of the pyrimidine H9 peak is observed at high temperatures (Figure 7). Since these doublets all have different J values, they do not arise from couplings between the ring protons. Past analogue studies[12] indicated that the imidazole protons of the $[Co(PMA)]^{2+}$ moiety are very sensitive to its surrounding electron density. The splitting of specific resonances of the PMA^- framework in **7**−**9** (1:1) likely arises from the diastereomeric complexes formed upon the electrostatic association of the Λ and Δ isomers of the $[Co(PMA)]^{2+}$ moiety of **7** with **9**. Such resolution of proton resonances for Λ and Δ isomers

Table 3. Summary of NOEs Observed between [Co(PMA)(Int-A)]$(NO_3)_2$ (**7**) and d[GATCCGGATC]$_2$ (**9**) at 25 and 50 °C

Intermolecular NOEs between **7** and **9** at 25 °C					
6.95 ppm acridine peaks			7.34 ppm acridine peaks		
9	ppm	intensity	**9**	ppm	intensity
G6H1′	5.46	s	T9CH$_3$	1.36	m
C4H5	5.47	s	T3CH$_3$	1.37	m
C5H5	5.55	s	G7H2′	2.60	w
G7H1′	5.57	s	G7H2″	2.67	w
G7H8	7.73	s			
G6H8	7.77	s			
T3H1′	5.93	m			
A2H8	8.26	m			
A8H8	8.14	m			
T3CH$_3$	1.37	m			
T9CH$_3$	1.36	m			
A8H1′	6.17	w			
A2H1′	6.25	w			
G7H2′	2.60	w			
G6H2″	2.72	w			

Intermolecular NOEs between **7** and **9** at 50 °C					
6.98−7.05 ppm acridine peaks			7.34−7.36 ppm acridine peaks		
9	ppm	intensity	**9**	ppm	intensity
G6H8	7.75	s	G6H2″	2.67	m
G7H1′	5.58	s	A8H2″	2.84	m
C4H1′	5.93	s			
G6H1′	5.49	s			
A8H1′	6.20	m			
A2H1′	6.26	m			

upon DNA binding has been observed in the work of Barton *et al.* with octahedral tris(polypyridyl)metal complexes.[38] That the enantioselective interaction results from electrostatic binding of the $[Co(PMA)]^{2+}$ moiety of **7** to the duplex **9** is further supported by the observation that under high-salt condition (Figure 6), the pyrimidine H9 moves back to its position in free **7** (9.17 ppm) and the imidazole H1 doublet collapses into a singlet at 8.51 ppm (position in free **7**). This interaction is evident even at 50 °C. Also, though recognizable downfield shifts for H2, H4, and H9 of the PMA^- framework are noted with the **7**−**9** (1:1) complex, no distinct intermolecular NOEs between these protons and the protons of **9** are observed. Taken together, the result of the high-salt experiment and the absence of intermolecular NOEs between the PMA^- ligand framework and **9** indicate that, in **7**−**9** (1:1), the $[Co(PMA)]^{2+}$ moiety of **7** resides in close proximity to the phosphate backbone of the duplex (i.e. electrostatic interaction).

Our results imply that only one enantiomer of **7** is able to interact electrostatically with **9**. This is clearly evident in the way the chemical shifts of the imidazole H1 change upon binding to **9**. In **7**−**9** (1:1) complex, one of the two H1 resonances is shifted upfield (8.46 ppm) while the other peak remains at the position (8.51 ppm) noted for free **7**. Furthermore, it is the shifted resonance at 8.46 ppm which moves back to 8.51 ppm upon addition of NaCl. Interestingly, in the work of Barton *et al.*, the resonances of both Λ and Δ enantiomers of $[M(phen)_3]^{n+}$ shift upon DNA binding; however, in these cases, both enantiomers are associated with DNA in specific manners. In the present case, the bifunctional binding property of **7** (intercalative and electrostatic) presumably allows only one of the enantiomers to interact with **9** electrostatically.

It is known that intercalation of small ligands does not perturb the resonances of the DNA protons to a great extent.[29] This explains the relatively small shifts noted for the resonances of **9** in the **7**−**9** (1:1) complex (Table 1). Modest shifts upon

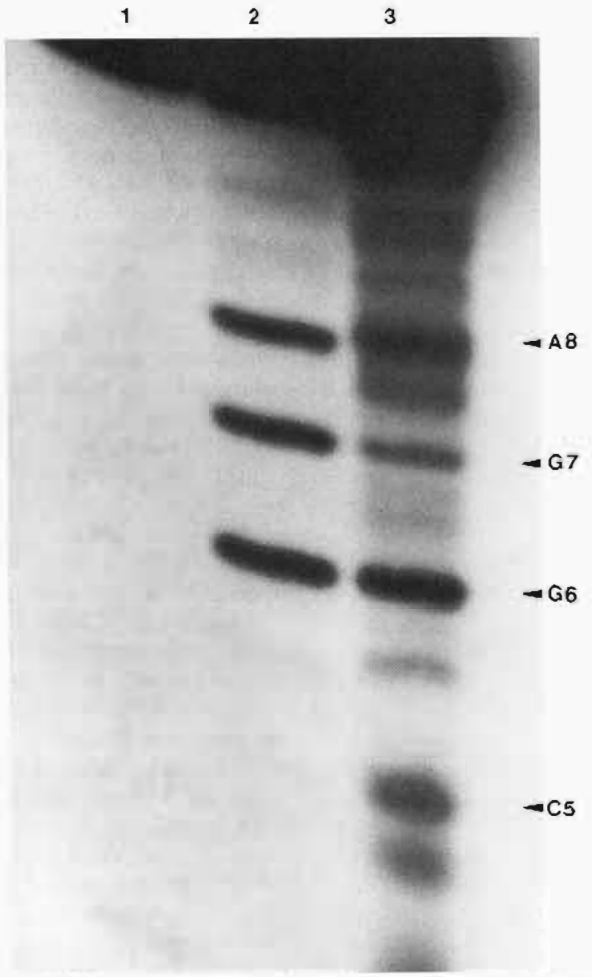

Figure 10. Sequence dependent photocleavage of the 5′-end labeled d[GATCCGGATC]$_2$ (**9**): lane 1, 50 pmol of 5′-end labeled **9** together with 1 mg of **9** as cold carrier in a total volume of 25 μL of 25 mM Tris−borate, 190 μM EDTA (pH = 8) buffer; lane 2, Maxam−Gilbert A+G reaction products; lane 3, same as lane 1 plus 30 μM of [Co(PMA)(Int-A)]Cl_2 (**7**). The samples were irradiated at 290 nm for 12 h at 4 °C.

complexation of **7** to **9** are observed with the bases G7, G6, C5, and C4. In contrast, the resonances of the acridine moiety of **7** shift quite considerably upon intercalation into **9**. The upfield shifts of the acridine protons H23−H32 confirm that the heterocyclic ring system intercalates into the duplex.[37] Furthermore, the acridine resonances get divided into two sets. Half of the acridine protons, as determined by area integration, are more broad and shifted more upfield compared to the other half. This observation along with the results of the temperature dependence (Figure 7) and NOE studies (Figures 8 and 9) indicates that (a) the intercalating acridine is in intermediate exchange regime at 25 °C and (b) the outer half (the side of the heteroatom) of the acridine containing H25, H26, H29, and H30 remains "inside" the duplex more often than the inner half bearing H23, H24, H31, and H32.

2D NMR spectroscopy has been used successfully to study DNA−drug interactions in solution.[38−45] We have employed

(38) Rehmann, J. P.; Barton, J. K. *Biochemistry* **1990**, *29*, 1701−1709.

(39) (a) David, S. S.; Barton, J. K. *J. Am. Chem. Soc.* **1993**, *115*, 2984−2985. (b) Mrksich, M.; Wade, W. S.; Dwyer, T. J.; Geierstanger, B. H.; Wemmer, D. E.; Dervan, P. B. *Proc. Natl. Acad. Sci. U.S.A.* **1992**, *89*, 7586−7590.

(40) Liu, X.; Chen, H.; Patel, D. J. *J. Biomol. NMR* **1991**, *1*, 323−347.

(41) Kumar, S.; Yadagiri, B.; Joseph, T.; Pon, R. T.; Lown, J. W. *J. Biomol. Struc. Dyn.* **1991**, *9*, 1,1−21.

(42) Pothier, J.; Delepierre, M.; Barsi, M.-C.; Garbay-Jaureguiberry, C.; Igolen, J.; Le Bret, M.; Roques, B. P. *Biopolymers* **1991**, *31*, 1309−1323.

this technique to study in detail the characteristics of the binding of the hybrid molecule **7** to the designed self-complementary decamer **9**. In all 2D spectra of **7**−**9** (1:1), the acridine protons exhibit strong NOEs to sugar H1′, H2′−H2″ and the aromatic base protons in the G6—G7 and the C4—C5 regions. Important is to note the correlations that exist for the acridine peaks in the 6.95 ppm region with G7H2′ and G6H2″. The G6H2″ sugar proton is on the same side as the 3′-OH while the G7H2′ sugar proton resides on the same side as the 5′-CH_2OH. It is thus clear that the acridine moiety shows NOEs to the duplex protons in a manner analogous to those observed for a base pair to its neighboring base pair and sugar protons. This is strong evidence for intercalation primarily at the G6—G7 step. That this intercalation occurs from the major groove side is indicated by a number of NOEs between the acridine protons and the base protons in the major groove (CH5, GH8, and the TCH_3s). The most compelling evidence is provided by the moderately strong NOEs observed between the acridine protons in the 7.34 ppm region (belonging to the inner half of the acridine that is connected to the $[Co(PMA)]^{2+}$ unit) and $T9CH_3$ and $T3CH_3$. These NOEs can only arise from intercalative interaction in the major groove since the methyl groups point out in the major groove of B-DNA.

Results of the photocleavage experiments with the end-labeled restriction fragments reveal that **7** binds preferentially to the G-rich regions and induce strand scission at 5′GG—N3′ sites. Molecular modeling of the **7**−**9** (1:1) complex indicates that if the acridine moiety of **7** intercalates into the GG step of **9**, the $[Co(PMA)]^{2+}$ unit is able to electrostatically bind to the phosphate backbone at points one base pair away from the GG site. Furthermore, if the $[Co(PMA)]^{2+}$ unit is positioned close to the phosphate backbone, the acridine ring system fails to completely intercalate into the GG step and only the outer half of the acridine rings (the side where N resides) stays within the base pair. The other half is off the base stack due to the restraint from the tether. Figure 10 supports these inferences. Major strand scission is noted at A8, G6 and C5 when **7**−**9** (1:1) is incubated under UV illumination. Binding of **7** to **9** and the major cleavage sites are schematically illustrated in Scheme 1.

Scheme 1. Proposed Mode of Binding of **7** to **9** and the Cleavage Sites

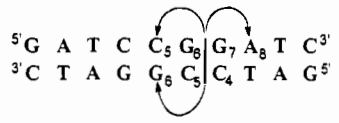

It is important to note here that though the concentrations of **7** and **9** in the photocleavage studies are very different (micromolar range) from those in the NMR experiments (millimolar range), the conclusions regarding the binding and photocleavage characteristics of **7** apply to both sets of experiments. Unfortunately, the details of the binding mode of **8** to **9** could not be studied by NMR due to very poor solubility of **8** in water. The results of the sequence specificity studies (Figure 1) indicate that the neutral Int-A (**8**) molecule fails to selectively intercalate into certain sites long enough to cause site specific photocleavage (only random cuts are observed). The combined effects of intercalation by the acridine moiety and electrostatic binding of the positively charged $[Co(PMA)]^{2+}$ unit, however, allow the hybrid molecule **7** to bind to certain sites more tightly and induce sequence specific photocleavage. Clearly, some kind of cooperativity in DNA binding has emerged from the attachment of the acridine (an intercalator) to the $[Co(PMA)]^{2+}$ core, a reagent for photoinduced DNA cleavage. At this time, syntheses and characterizations of more designed molecules are in progress in this laboratory. This tailored species will be utilized to test the hypothesis of cooperativity in this type of hybrid molecules.

Acknowledgment. This research was supported by grants from the American Cancer Society (CH-481) and the National Institute of Health (CA 53076-01). S.S.D. gratefully acknowledges support from the Arnold and Mabel Beckman Foundation. Purchase of the 500-MHz NMR spectrometer was made possible by a grant from the Markey Foundation. Experimental assistance from Mr. Jim Loo is gratefully acknowledged.

(43) Kumar, S.; Jasija, M.; Zimmermann, J.; Yadagiri, B.; Pon, R. T.; Sapse, A.-M.; Lown, J. W. *J. Biomol. Struct. Dyn.* **1990**, *8*, **1**, 99−121.
(44) Gao, X.; Patel, D. J. *Biochemistry* **1989**, *28*, 751−762.
(45) Patel, D. J.; Shapiro, L. *J. Biol. Chem.* **1986**, *261*, **3**, 1230−1240.